www.czasopisma.pan.pl PAN POLSKA AKADEMIA NAUK www.journals.pan.pl

Metrol. Meas. Syst., Vol. 24 (2017), No. 3, pp. 515–524.

PAN POLSKA AKADEMIA NAUK

METROLOGY AND MEASUREMENT SYSTEMS

Index 330930, ISSN 0860-8229

www.metrology.pg.gda.pl

M&MS

MEASUREMENT AND ANALYSIS OF PARTIAL DISCHARGE USING AN ULTRA-HIGH FREQUENCY SENSOR FOR GAS INSULATED STRUCTURES

Guoming Wang, Gyung-Suk Kil

Korea Maritime and Ocean University, Department of Electrical and Electronics Engineering, 727, Taejong-ro, Yeongdo-gu, Busan, Korea (journey@kmou.ac.kr, ✉ kilgs@kmou.ac.kr, +82 51 410 4414)

Abstract

Although the gas insulated structures have a high degree of reliability, the unavoidable defects are primary reason of their failures. *Partial discharge* (PD) has been regarded as an effective indication for condition monitoring and diagnosis of *gas insulated switchgears* (GISs) to ensure their reliable and stable operation. Among various PD detection methods, the *ultra-high frequency* (UHF) technique has the advantages of on-line motoring and defect classification. In this paper, there are presented 7 types of artificial electrode systems fabricated for simulation of real insulation defects in gas insulated structures. A real-time measurement system was developed to acquire defect patterns in a form of *phase-resolve partial discharge* (PRPD) intensity graph, using a UHF sensor. Further, the discharge distribution and statistical characteristics were extracted for defect identification using a neural network algorithm. In addition, a conversion experiment was proposed by detecting the PD pulse simultaneously using a non-induction resistor and a UHF sensor. A relationship between the magnitude of UHF signal and the amplitude of apparent charge was established, which was used for evaluation of PD using the UHF sensor.

Keywords: gas insulated structures, partial discharge, ultra-high frequency sensor, conversion.

1. Introduction

The gas insulated structures that are filled with sulphur hexafluoride (SF_6) gas, such as switchgears and transmission lines, have a high insulation and arc-extinguishing capability, ensuring their high reliability, compact size, and economical efficiency. As a result, they are widely employed in space-limited locations, such as city substations, offshore plants, and electric railway systems. The *gas insulated switchgears* (GISs), which are composed of a circuit breaker, disconnect and grounding switches and other high voltage components, have been used for power transmission and distribution sine 1960s. In addition, a *gas insulated transmission line* (GIL) is regarded as a safe and flexible alternative to an overhead line. However, insulation defects generated during the manufacture, assembly, transportation and operation are one of the primary causes of GIS and GIL failures [1–4]. Owing to the large power supply capacity, the failures result in enormous economic losses and serious human injuries. It is therefore necessary to monitor and diagnose the condition of gas insulated structures to work out proper maintenance schedules and to ensure their reliable and stable operation [5–6].

The maintenance strategy for power facilities has developed from the run-to-failure, through the maintenance as necessary, time-based and condition-based maintenance, to the *reliability-centred maintenance* (RCM) that is proposed nowadays. The RCM strategy is a combination of the reactive, preventive, predictive, and proactive maintenance to maximise the reliability and availability of power apparatus [7–8]. The *partial discharge* (PD) is defined as a localized electrical discharge that partially bridges the insulation [9–10]. It causes progressive deterioration and the final failure of equipment. Therefore, monitoring and analysis of PD are important parts of RCM. The study of PD consists of four parts: detection, analysis,

Article history: received on Dec. 03, 2016; accepted on Feb. 26, 2017; available online on Sep. 01, 2017; DOI: 10.1515/mms-2017-0045.

classification, and localization [11]. PD detection methods are categorized into the conventional and non-conventional ones. A conventional method is a means of measuring the electrical discharge pulse, complying with IEC 60270 [9]. Non-conventional ways of detection include acoustic emission, dissolved gas analysis, and *ultra-high frequency* (UHF) methods [12–19]. Among various methods, UHF is the best choice including the four mentioned activities. In addition, it has obvious advantages of immunity against external noise and the capability of on-line monitoring [20–21].

This paper discusses the measurement and analysis of PD using a UHF sensor for condition monitoring and diagnosis of gas insulated structures. All of the possible insulation defects in GIS were simulated. A real-time analysis system was developed to extract *phase-resolved partial discharge* (PRPD) patterns and to identify a defect type using 17 proposed parameters. In addition, a conversion method was proposed to analyse the relationship between the magnitude of UHF signal and the amplitude of apparent charge, used for evaluation of PD with the non-conventional UHF method.

2. Experiment

2.1. Insulation defects

PD occurs in an insulation defect that is generated during the manufacture, assembly, and transportation procedures of gas insulated structures. Most of such defects can be detected in the factory and commissioning tests whereas there are still some micro ones hard to be found. Left without checking, those micro defects cause a progressive deterioration of the dielectric material even though power facilities operate at their rated voltage [22]. Fig. 1 shows 7 types of typical insulation defects in GIS and GIL, including *protrusion on conductor* (POC), *protrusion on enclosure* (POE), *void inside spacer* (VIS), *particle on spacer* (POS), *crack inside spacer* (CIS), *free particle* (FP), and floating. In this paper, they were simulated using artificial defects.

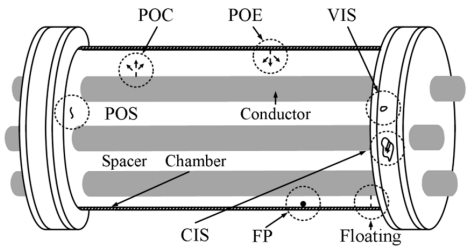

Fig. 1. Typical insulation defects in GIS and GIL.

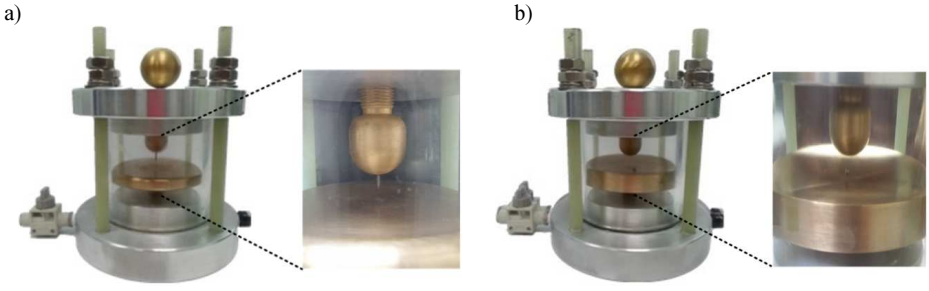

Fig. 2. Examples of artificial defects: protrusion on conductor (a); free particle (b).

Metrol. Meas. Syst., Vol. 24 (2017), No. 3, pp. 515–524.

Examples of the POC and FP defects are illustrated in Fig. 2. In the POC and POE, a needle electrode with a curvature radius of 5 μm representing a micro-size metallic protrusion, and a plane electrode with a diameter of 80 mm were used. A distance between the two electrodes was 3 mm. The edge of the plane electrode was rounded to prevent concentration of the electric field. The VIS, POS, and CIS were designed to simulate deficiencies in the spacer of GIS or GIL, representing an imperfection of product, attachment of a conductive particle, and a crack resulting from impact, respectively. The FP, which is the most common defect, was created as a 1 mm-diameter aluminium sphere to simulate a free moving metal in the chamber. All of the artificial defects were sealed with SF_6 gas with a pressure of 0.5 MPa.

2.2. Measurement system

The measurement program was developed using a real-time operation system based on LabVIEW. Fig. 3 demonstrates a flow chart of the measurement system. The virtual instruments (VI) were divided into HOST VI that runs on a personal computer, and RT VI that operates on a PXI. The shared variables were used for communication between those two VIs.

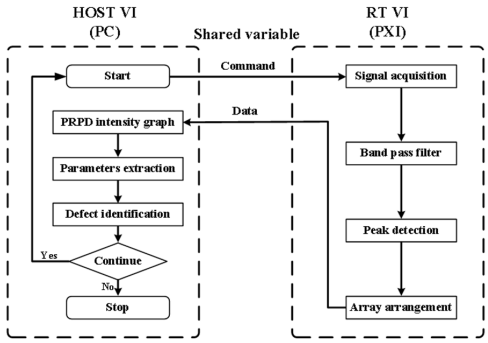

Fig. 3. A flow chart of the measurement system.

In the RT VI, a producer-consumer design pattern based on queue operation was applied, which is able to run the application with precise timing and a high degree of reliability. The acquired signal was then fed through a band-pass filter to suppress the mobile telephone interference at a frequency of 800–900 MHz. The peak point of UHF signal was captured by peak detection to be displayed in the PRPD intensity graph. The arranged data were sent to the personal computer for further analysis.

In the HOST VI, a standard state machine design pattern was built, which enabled distinct states to operate in a programmatically determined dynamic sequence. The following parameters: pulse distribution, skewness, kurtosis, and *correlation coefficient* (CC), were extracted.

The skewness and kurtosis are given by:

$$Skewness = \sum_{i=1}^{n} \frac{[X(i)-\mu]^3}{n\times\sigma^3}, \tag{1}$$

$$Kurtosis = \sum_{i=1}^{n} \frac{[X(i)-\mu]^4}{n\times\sigma^4}, \tag{2}$$

where: $X(i)(i = 1, 2,..,n)$ are data sets; μ and σ are their means and standard deviations, respectively. In the present study, $X(i)$ are the PRPD data in the positive or negative half of the applied voltage. Skewness is a measure of the symmetry of a distribution in respect of the normal distribution. The negative values of skewness indicate data that are left-skewed, whereas positive values indicate right-skewed data. The symmetric data which are called

a normal distribution have a skewness value of zero. Kurtosis is an indicator of the steepness of a probability distribution. The normal distribution has a kurtosis value of 3. The data with a kurtosis value higher than 3 tend to be steeply distributed, whereas the data with a kurtosis value lower than 3 tend to be distributed evenly.

The correlation coefficient that is used to evaluate the similarity of two signals is calculated as follows:

$$CC = \frac{\sum_{i=0}^{n-1}\{[X(i)-\bar{X}]\times[Y(i)-\bar{Y}]\}}{\sqrt{\sum_{i=0}^{n-1}\{[X(i)-\bar{X}]^2\times[Y(i)-\bar{Y}]^2\}}}, \tag{3}$$

where: $X(i)$ and $Y(i)$ are two data sets; and $\bar{X}$ and $\bar{Y}$ are their average values. To be specific, $X(i)$ and $Y(i)$ are the PRPD data in the positive and negative halves of applied voltage, respectively. A value of CC is between 0 and 1. A large value indicates a high similarity of two signals [23–24]. Finally, the extracted parameters were input into a neural network for classifying the type of defect.

2.3. Experimental setup

The experimental setup is shown in Fig. 4. A dry-type transformer with a maximum output of 50 kV was immersed in insulation oil to avoid the occurrence of corona. The applied voltage was measured by a high voltage capacitive divider. Its capacitance and ratio were 25 pF and 10,000:1, respectively. An artificial defect was placed inside a GIS chamber to generate PD pulses. A UHF sensor with a frequency range of 0.5–1.5 GHz was mounted in a window of GIS. It is a semi-circular dipole antenna with a minimum detection sensitivity of 1 *pico-coulombs* (pC). To verify the validity of the developed measurement system and to run the conversion experiment, a 50 Ω non-inductive resistor was connected to detect a PD pulse. The signal was acquired using a *digital storage oscilloscope* (DSO) with a sampling rate of 5 GS/s and a *data acquisition* (DAQ) unit with a sampling rate of 250 MS/s.

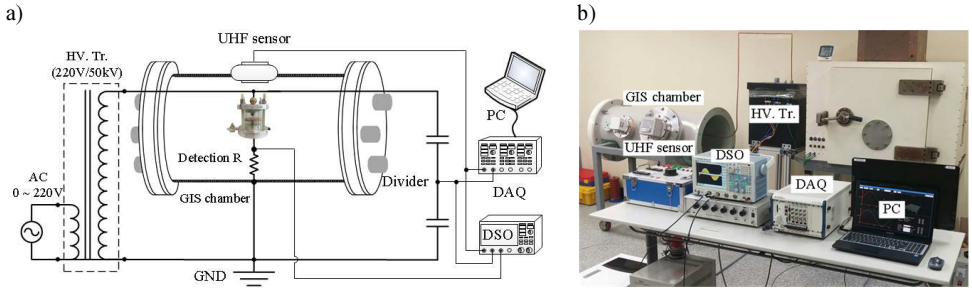

Fig. 4. The experimental setup: a configuration (a); a photograph (b).

3. PRPD and defect classification

Depending on the types of defects, PD presents different patterns. The parameters extracted from PD patterns are used for identification of defects; basing on these parameters the operating personnel can work out a proper maintenance schedule for the in-service equipment. In this section, the PRPD intensity graphs that feature the φ-q-n pattern were acquired from seven types of artificial defects, where φ is a phase position, q is a discharge magnitude, and n is a count of PD events. An intensity graph was acquired from the PXI using the UHF sensor and was simultaneously collected by the DSO through the resistor. These two graphs were compared to verify the validity of the proposed measurement system. To reduce the complexity of PD patterns, characteristic properties were analysed regarding distribution of pulses and statistical

Metrol. Meas. Syst., Vol. 24 (2017), No. 3, pp. 515–524.

features. For the distribution of pulses, a PRPD intensity graph was divided into 12 windows and percentages of PD pulses in each window were calculated, named P1, P2,…, P12, as illustrated later. The statistical features include the skewness and kurtosis of the phase spectra in the positive and negative halves of applied voltage, as well as the *CC* value between the phase spectra in the positive and negative halves. Finally, the 17 extracted parameters were input into the artificial neural network for classifying the type of defect.

The PRPD intensity graphs of POC acquired from the DSO and the measurement system are shown in Fig. 5. It can be seen that the same pattern was obtained. PD pulses are distributed in 33–108° in the positive half of applied voltage and in 140–305° in the negative half. The magnitudes of pulses in the positive half were higher than those in the negative half. In addition, the counts of pulses in the positive and negative halves were 509 and 253, respectively. Fig. 6 demonstrates the PRPD distribution as well as the phase spectrum. 99.5% of PD pulses are in the positive half. Especially, 51.69% of pulses are clustered in the window of 90–180° and −60 – −80 dBm. Further, the statistical parameters were extracted from the phase spectrum.

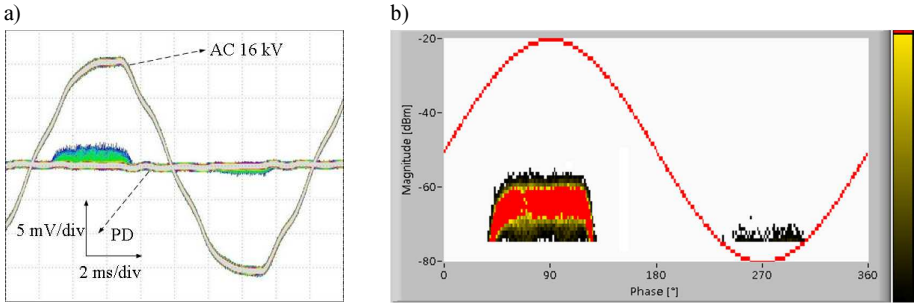

Fig. 5. A PRPD intensity graph of POC: DSO (a); the measurement system (b).

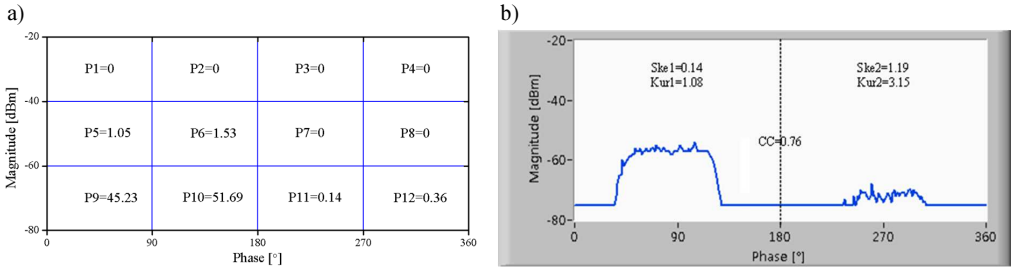

Fig. 6. Parameters of POC: a PRPD distribution (a); a phase spectrum (b).

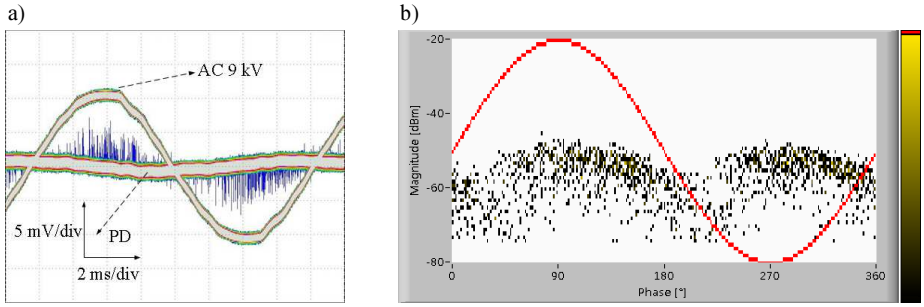

Fig. 7. A PRPD intensity graph of FP: DSO (a); the measurement system (b).

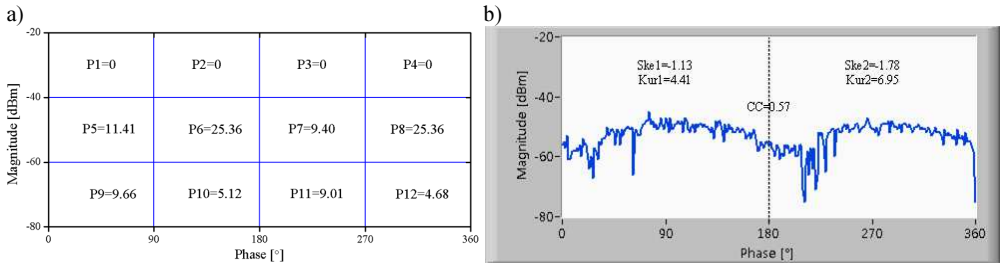

Fig. 8. Parameters of FP: a PRPD distribution (a); a phase spectrum (b).

Figures 7 and 8 illustrate the PRPD intensity graph and parameters of FP, respectively. Pulses scattered over all of the phase and the discharge magnitude varied with the amplitude of applied voltage. The discharge patterns were similar in the positive and negative halves.

The PRPD intensity graphs and parameters of other five types of defects are appended. In the POE, most of PD pulses are distributed in the negative half of applied voltage, and the magnitudes of pulses in the negative half are higher than those in the positive half. Similar patterns in the positive and negative halves were acquired in the VIS, where pulses are distributed within 30°–90° and 210°–270°. In the POS, PDs occurred with a magnitude lower than −62 dBm, whereas PD pulses with a magnitude higher than −30 dBm were detected in the floating. In the CIS, most of pulses are distributed in the P9 and P11 windows.

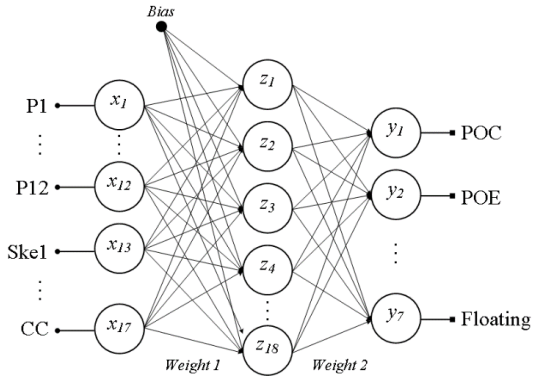

Fig. 9. A structure of artificial neural network.

A structure of artificial neural network is demonstrated in Fig. 9. There are 17 neurons – as many as the number of extracted parameters in the input layer. One hidden layer with 18 neurons was used to connect the neurons in the input and output layers. The number of neurons in the output layer is the same as that of the typical insulation defects, which is set to 7. In addition, a sigmoid function is selected to determine the activation function. During the training procedure, the PRPD intensity graphs had been extracted for 20 times from each defect and a back propagation algorithm was applied to update the weights and biases until the allowable error was less than 0.0001. Then, the updated weights and biases were written into the measurement system to replace their initial values; they were finally used for real-time defect identification. To verify the accuracy of the developed system, another 20 groups were acquired for each of 7 defects, and then identified. As a result, 134 of 140 data were accurately identified. Therefore, the proposed system can classify a defect type with an average accuracy of 95.7%.

Metrol. Meas. Syst., Vol. 24 (2017), No. 3, pp. 515–524.

4. Apparent charge calculation

In IEC 60270, PD is evaluated using an apparent charge (q), whose unit is pC [9]. The apparent charge is an integrated value of the detected pulse and can be calculated by:

$$q = \int_{t_1}^{t_2} i(t)dt = \int_{t_1}^{t_2} \frac{v(t)}{50} dt \quad [\text{pC}], \tag{4}$$

where: $v(t)$ is a waveform of pulse detected by the non-inductive resistor. The accuracy was verified by injecting current pulses with specified apparent charges using a calibrator, and then comparing the injected values with the integrated ones. The magnitude of UHF signal is expressed in dBm. The conversion experiment was performed to analyse the relationship between the magnitude of UHF signal and the apparent charge, in order to evaluate PD with UHF sensors. Fig. 10 shows electrical PD pulses simultaneously measured with the UHF signals. Since a UHF pulse lasts only tens of nanoseconds, an extremely expensive acquisition device with a high sampling rate is needed to capture such a short signal. Therefore, an integral circuit was used in this sensor. As a result, the width of pulse detected with the UHF sensor (lower) was longer than that detected by the 50 Ω resistor (upper). It can be seen that PD pulses detected by the resistor and the UHF sensor matched very well, providing the evidence for a good conversion accuracy.

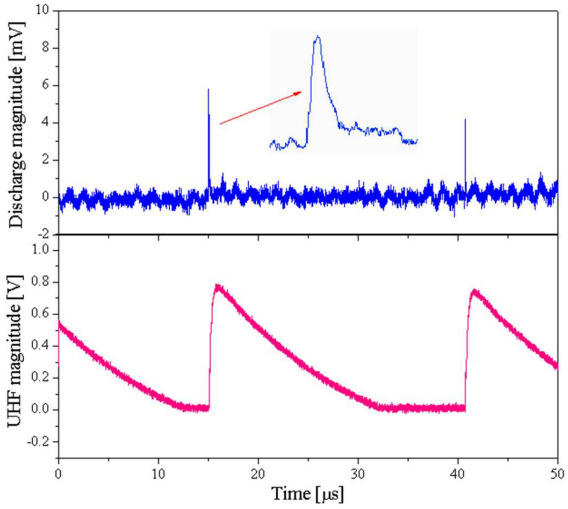

Fig. 10. PD pulses detected by the 50 Ω resistor (upper) and the UHF sensor (lower).

The conversion experiment was carried out for 7 defects. The results are shown in Fig. 11. Although obtained for different defect types, the relationships between the magnitude of UHF signal and the amplitude of discharge follow a single curve, which is given in (5). Therefore, the dBm can be converted into pC for evaluating PD by the UHF sensor during the on-line PD monitoring:

$$q = 10^{\frac{mangitude\ of\ UHF\ signal\ in\ dBm + 81.31}{23.32}} \quad [\text{pC}]\ . \tag{5}$$

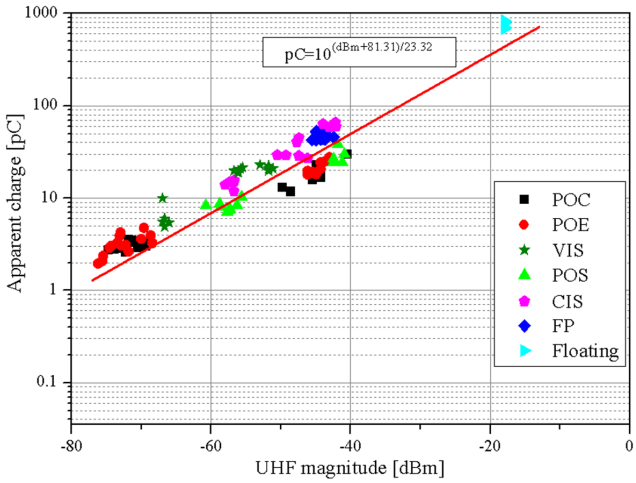

Fig. 11. The results of conversion.

5. Conclusions

This paper deals with the measurement and analysis of PD using a UHF sensor for the purpose of condition monitoring and diagnosis of gas insulated structures. A real-time measurement system that combined the signal acquisition, pattern generation, feature extraction and defect identification was developed. The PRPD intensity graphs were acquired from 7 types of artificial defects, which presented distinguishable patterns. Then, 17 parameters were extracted, including the distribution of PD pulses over 12 phase-magnitude windows, skewness and kurtosis of the phase spectra in the positive and negative halves of applied voltage, as well as the correlation coefficient between the phase spectra in the positive and negative halves. Using an artificial neural network, the defects were classified with a high accuracy of 95.7%. In addition, by using the proposed conversion method, the relationship between the magnitude of UHF signal and the amplitude of apparent charge was examined, even for different defects. Therefore, PD can be evaluated using a UHF sensor in the gas insulated structures in service.

References

[1] Haddad, A., Warne, D.F. (2004). *Advances in high voltage engineering*. The Institution of Engineering and Technology, 37–54.

[2] Ryan, H.M. (2013). *High-voltage engineering and testing*. The Institution of Engineering and Technology, 319–324.

[3] Neumann, C., Krampe, B., Feger, R., Feser, K., Knapp, M., Breuer, A., Rees, V. (2000). PD measurements on GIS of different designs by non-conventional UHF sensors. *CIGER session 15–305*, 1–9.

[4] ABB. (2009). Compact and reliable – Decades of benefits: Gas-insulated switchgear from 52 to 1100 kV (ABB Technology magazine), 1–7.

[5] Neumann, C., Rusek, B., Balzer, G., Jeromin, I. (2012). End of life estimation and optimisation of maintenance of HV switchgear and GIS substations. *CIGER session A3–202*, 1–12.

[6] Jo, H.E., Wang, G.M., Kim, S.J., Kil, G.S. (2015). Comparison of partial discharge characteristics in SF_6 gas under AC and DC. *Trans. Electr. Electron. Mater.*, 16(6), 323–327.

[7] Gill, P. (2008). *Electrical power equipment maintenance and testing*. CRC Press, 1–18.

Metrol. Meas. Syst., Vol. 24 (2017), No. 3, pp. 515–524.

[8] Balzer, G., Degen, W., Halfmann, M., Hartkopf, T., Neumann, C. (2004). Strategies for optimizing the use of substation assets. *CIGER session B3–101*, 1–8.

[9] IEC 60270. (2000). *High-voltage test techniques-Partial discharge measurement.*

[10] Tang, J., Xie, Y. (2011). Partial discharge location based on time difference of energy accumulation curve of multiple signals. *IET Electr. Power Appl.*, 5(1), 175–180.

[11] Kreuger, F.H. (1990). *Partial discharge detection in high-voltage equipment*. Butterworths, 29–48.

[12] Vedral. J., Kříž, M. (2010). Signal processing in partial discharge measurement. *Metrol. Meas. Syst.*, 31(6), 22–35.

[13] IEEE. (2007). IEEE guide for the detection and location of acoustic emission from partial discharges in oil-immersed power transformers and reactors.

[14] Hekmati, A. (2016). A novel acoustic method of partial discharge allocation considering structure-borne waves. *Int. J. Electr. Power Energy Syst.*, 77, 250–255.

[15] Kil, G.S., Kim, I.K., Park, D.W., Choi, S.Y., Park, C.Y., (2009). Measurements and analysis of the acoustic signals produced by partial discharge in insulation oil. *Curr. Appl. Phys.*, 9(2), 296–300.

[16] Kim, S.W., Kim, S.J., Seo, H.D., Jung, J.R., Yang, G.J., Duval, M. (2013). New methods of DGA diagnosis using IEC TC 10 and related databases part 1 application of gas-ratio combinations. *IEEE Trans. Dielect. Elect. Insul.*, 20(2), 685–690.

[17] Muhamad, N.A., Phung, B.T., Blackburn, T.R. (2011). Dissolved gas analysis for common transformer faults in soy seed-based oil. *IET Electr. Power Appl.*, 5(1), 133–142.

[18] Zhu, M.X., Xue, J.Y., Zhang, J.N., Li, Y., Deng, J.B., Mu, H.B., Zhang, G.J., Shao, X.J., Liu, X.W. (2016). Classification and separation of partial discharge ultra-high-frequency signals in a 252 kV gas insulated substation by using cumulative energy technique. *IET Sci. Meas. Technol.*, 10(4), 316–326.

[19] Raja, K., Devaux, F., Lelaidier, S. (2002). Recognition of discharge sources using UHF PD signatures. *IEEE Elect. Insul. Mag.*, 18(5), 8–14.

[20] Wang, Y.C., Wu, J.D., Li, Z., Yin, Y. (2014). Research on a practical de-nosing method and the characterization of partial discharge UHF signals. *IEEE Trans. Dielect. Elect. Insul.*, 21(5), 2206–2216.

[21] Okabe, S., Ueta, G., Hama, H., Ito. T., Hikita, M., Okubo, H. (2014). New aspects of UHF PD diagnostics on gas-insulated systems. *IEEE Trans. Dielect. Elect. Insul.*, 21(5), 2245–2258.

[22] CIGER. (2013). *Risk assessment on defects in GIS based on PD Diagnosis*.

[23] Sahoo, N.C., Salama, M.M.A., Bartnikas, R. (2005). Trends in partial discharge pattern classification: A survey. *IEEE Trans. Dielect. Elect. Insul.*, 12(2), 248–264.

[24] Masud, A.A., Stewart, B.G., Mcmeekin, S.G. (2014). Application of an ensemble neural network for classifying partial discharge patterns. *Electr. Power Syst. Res.*, 110, 154–162 .

Appendices

Figures 12−16 show the PRPD intensity graphs and parameters of five types of defects.

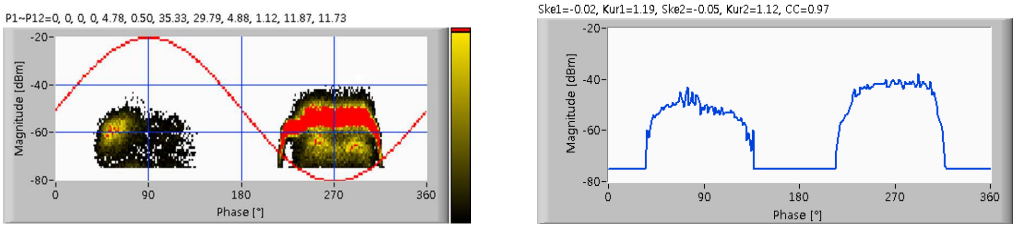

Fig. 12. PRPD intensity graph and parameter of protrusion on enclosure.

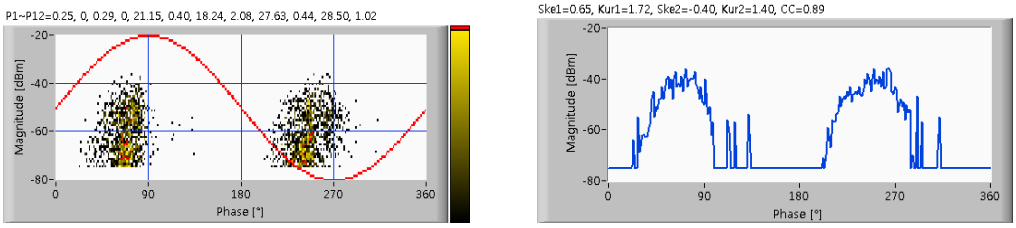

Fig. 13. PRPD intensity graph and parameter of void inside spacer.

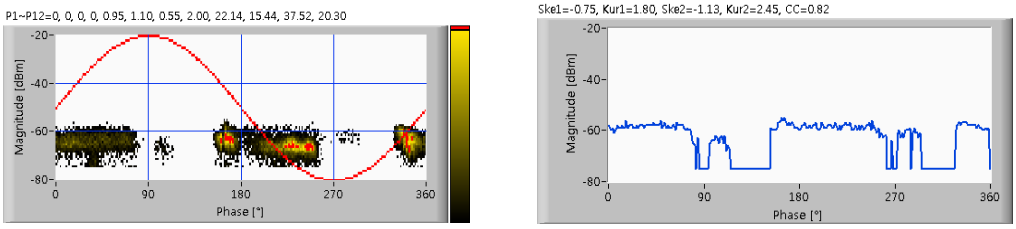

Fig. 14. PRPD intensity graph and parameter of particle on spacer.

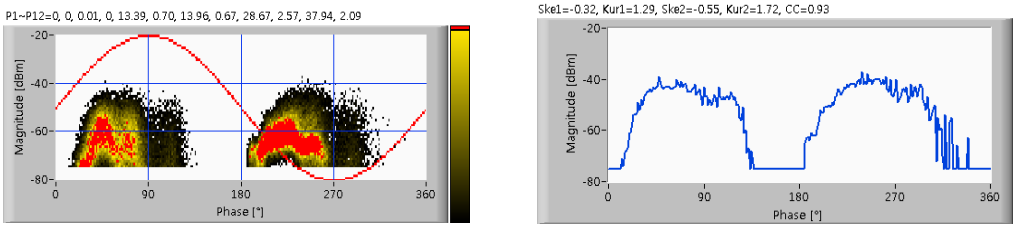

Fig. 15. PRPD intensity graph and parameter of crack inside spacer.

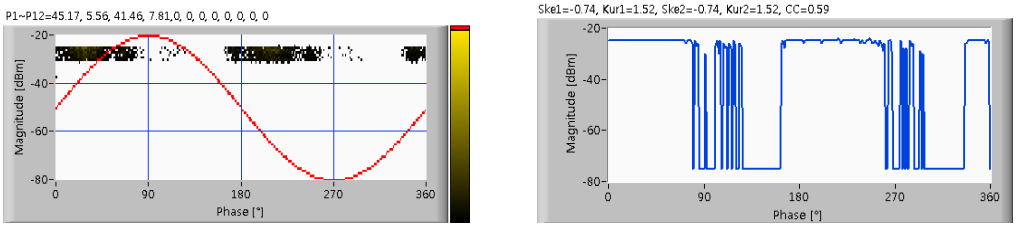

Fig. 16. PRPD intensity graph and parameter of floating.